



*Supplement of*

## **A predictive viscosity model for aqueous electrolytes and mixed organic–inorganic aerosol phases**

**Joseph Lilek and Andreas Zuend**

*Correspondence to:* Andreas Zuend ([andreas.zuend@mcgill.ca](mailto:andreas.zuend@mcgill.ca))

The copyright of individual parts of the supplement might differ from the article licence.

## S1 Derivation for cation–anion viscosity contribution weighting

This section further describes the cation–anion contribution treatment introduced in Section 2.3 of the main text. For multi-ion mixtures, a special weighting must be derived to be fully consistent with all potential cation–anion pairings and such that there is no double counting of the contributions of a specific ion when paired up with the various anions. This can be accomplished by treating the aqueous solution as a mixture of (dissolved) charge-neutral cation–anion pairs, with each cation combined with each anion proportionally to the charge-weighted ion amounts involved in the solution overall. That is, we can think of the ions present in the solution as being the result of dissolving various possible electrolyte components (initially). The goal here is to provide a means of quantifying a “fair” share of each possible electrolyte component (as a binary, charge-balanced cation–anion unit) in a clearly defined manner. Consider the total of positive charges in the aqueous electrolyte mixture,  $\sum_{c=1}^{J_c} n_c \cdot z_c$ , which is equivalent in magnitude to the total of negative charges,  $\sum_{a=1}^{J_a} n_a \cdot |z_a|$ , for an overall charge-neutral solution. We can define the charge fraction  $\psi_a$  as the absolute amount of charge contributed by anion  $a$  relative to the sum of absolute charge contributions from all negative charges present (or alternatively, relative to the sum of all positive ones) in the mixture,

$$\psi_a = \frac{n_a \cdot |z_a|}{\sum_{a'=1}^{J_a} n_{a'} \cdot |z_{a'}|}, \quad (\text{S1})$$

and introduce a cation–anion pair contribution weighting term,

$$\tau'_{c,a} = \frac{n_c}{\nu_{c,el}} \cdot \psi_a. \quad (\text{S2})$$

$\tau'_{c,a}$  represents the fractional amount of the hypothetical, neutral electrolyte component  $el$  consisting of cation  $c$  and anion  $a$ , where  $\nu_{c,el}$  is the stoichiometric number of cations in a formula unit of this electrolyte. Note that there is only one such cation–anion combination per specific type of cation and anion. In Eqs. (17 – 18),  $x_c$  can be understood as the molar amount of cation  $c$  in solution, normalized by the total molar amount of all species. Therefore, it is clear that either using an absolute, mole-based scaling ( $\tau'_{c,a}$ ) or a relative mole-fraction-based scaling ( $\tau_{c,a}$ , Eq. 18) offer a description of the amounts of each “input” electrolyte component contributing ions to a solution (or unit amount of solution). The prime notation is removed in Eqs. (17 – 18) to indicate that mole-fraction-based scaling is used.

To illustrate the utility and consistency of this approach, consider an example mixture containing 2 mol NaCl, 9 mol MgSO<sub>4</sub>, and 3 mol NaBr in water. If all these electrolytes completely dissociate (as is assumed by AIOMFAC), the resulting solution composition can be written as 5 mol Na<sup>+</sup>, 2 mol Cl<sup>−</sup>, 9 mol Mg<sup>2+</sup>, 9 mol SO<sub>4</sub><sup>2−</sup>, and 3 mol Br<sup>−</sup> in solution. From these two cations and three anions, the following six charge-neutral cation–anion pairs can be formed: NaCl, MgSO<sub>4</sub>, NaBr, MgCl<sub>2</sub>, Na<sub>2</sub>SO<sub>4</sub>, and MgBr<sub>2</sub>.

When describing the viscosity contributions from cation–anions pairs using Eq. (14), in order to avoid excessive weight being attributed to a certain ion pair, we advocate that one should strive for an unbiased representation of the solution by means of accounting for all possible contributions from cation–anion pairs in a charge-equivalent manner of weighting. As a counter-example, an excessive, unbalanced weighting would likely occur if one were to pair, e.g., all  $\text{Mg}^{2+}$  with all  $\text{SO}_4^{2-}$  present, thereby giving a relatively high weight to the  $c_{\text{Mg}^{2+}, \text{SO}_4^{2-}}$  parameter (Eq. 14) in the mixture viscosity calculation. This may bias this model prediction toward the viscosity of aqueous  $\text{MgSO}_4$  (at the same ionic strength) and the resulting value may be substantially different from a viscosity calculation involving a different choice of cation–anion pairing, such as if we had first combined all  $\text{Na}^+$  with  $\text{SO}_4^{2-}$  and only the remainder of sulfate with magnesium. Hence, the specific sequence of pairing the cations with the anions into hypothetical electrolyte components will lead to different viscosity predictions by the model (if several options are possible), making the prediction dependent on seemingly arbitrary choices and thereby ambiguous. Such ambiguity can be circumvented by introducing our  $\tau'_{c,a}$ -based weighting, in which a fractional amount of each cation is combined with a fractional amount of each anion, proportional to the charge-weighted amounts of the anions and the stoichiometry of the electrolyte unit formed.

In our example,  $\text{Na}^+$  is paired with all anions ( $\text{Cl}^-$ ,  $\text{SO}_4^{2-}$ ,  $\text{Br}^-$ ) in such a way that the largest fractional amount of  $\text{Na}^+$  is paired with  $\text{SO}_4^{2-}$ , the second-largest amount is paired with  $\text{Br}^-$ , and the smallest amount is paired with  $\text{Cl}^-$ . We can calculate the exact proportions for  $\text{Na}^+$  by computing the charge-based fractions for each counter-ion (anion) using Eq. (S1). Here,

$$\psi_{\text{Cl}^-} = \frac{n_{\text{Cl}^-} \cdot |z_{\text{Cl}^-}|}{\sum_{J_c} n_c \cdot z_c} = \frac{2 \cdot |-1|}{(5 \cdot 1) + (9 \cdot 2)} = \frac{2}{23} \quad (\text{S3})$$

$$\psi_{\text{Br}^-} = \frac{n_{\text{Br}^-} \cdot |z_{\text{Br}^-}|}{\sum_{J_c} n_c \cdot z_c} = \frac{3 \cdot |-1|}{(5 \cdot 1) + (9 \cdot 2)} = \frac{3}{23} \quad (\text{S4})$$

$$\psi_{\text{SO}_4^{2-}} = \frac{n_{\text{SO}_4^{2-}} \cdot |z_{\text{SO}_4^{2-}}|}{\sum_{J_c} n_c \cdot z_c} = \frac{9 \cdot |-2|}{(5 \cdot 1) + (9 \cdot 2)} = \frac{18}{23}, \quad (\text{S5})$$

while for each of the  $\text{Na}^+$ –anion pairs, Eq. (S2) yields

$$\tau'_{\text{Na}^+, \text{Cl}^-} = \frac{n_{\text{Na}^+}}{\nu_{\text{Na}^+, \text{NaCl}}} \cdot \psi_{\text{Cl}^-} = \frac{5 \text{ mol}}{1} \cdot \frac{2}{23} = \frac{10}{23} \text{ mol} \quad (\text{S6})$$

$$\tau'_{\text{Na}^+, \text{Br}^-} = \frac{n_{\text{Na}^+}}{\nu_{\text{Na}^+, \text{NaBr}}} \cdot \psi_{\text{Br}^-} = \frac{5 \text{ mol}}{1} \cdot \frac{3}{23} = \frac{15}{23} \text{ mol} \quad (\text{S7})$$

$$\tau'_{\text{Na}^+, \text{SO}_4^{2-}} = \frac{n_{\text{Na}^+}}{\nu_{\text{Na}^+, \text{Na}_2\text{SO}_4}} \cdot \psi_{\text{SO}_4^{2-}} = \frac{5 \text{ mol}}{2} \cdot \frac{18}{23} = \frac{45}{23} \text{ mol}. \quad (\text{S8})$$

The  $\tau'_{c,a}$  value can be calculated for the other five potential charge-neutral cation–anion pairs, yielding  $\tau'_{\text{Mg}^{2+}, \text{SO}_4^{2-}} = \frac{162}{23} \text{ mol}$ ,  $\tau'_{\text{Na}^+, \text{Br}^-} = \frac{15}{23} \text{ mol}$ ,  $\tau'_{\text{Na}^+, \text{SO}_4^{2-}} = \frac{45}{23} \text{ mol}$ ,  $\tau'_{\text{Mg}^{2+}, \text{Cl}^-} = \frac{18}{23} \text{ mol}$ , and  $\tau'_{\text{Mg}^{2+}, \text{Br}^-} = \frac{27}{23} \text{ mol}$ . These values add up in a way that is stoichiometrically consistent, e.g., extracting the  $\text{Na}^+$  amount from these hypothetical electrolyte component amounts yields  $\tau'_{\text{Na}^+, \text{Br}^-} + \tau'_{\text{Na}^+, \text{Cl}^-} + 2 \cdot \tau'_{\text{Na}^+, \text{SO}_4^{2-}} = \frac{15+10+90}{23} \text{ mol} = 5 \text{ mol Na}^+$ . In our implementation of this approach, the normalized, mole-fraction-based version of  $\tau_{c,a}$  is used directly in Eq. (16).

## S2 Computational efficiency of organic–inorganic mixing approaches

We tested the speed of the three mixing approaches, finding that the ZSR-style mixing approach takes approximately five to six times longer than aquelec or aquorg. Results are shown in Tables S1 and S2.

**Table S1.** Time elapsed for multi-run simulations of the AIOMFAC-VISC mixing approaches. Each trial consisted of 200,000 runs. See also Table S2.

Trial	aquelec	aquorg	ZSR
1	5.02 s	5.08 s	27.89 s
2	4.39 s	4.38 s	27.45 s
3	4.36 s	4.28 s	23.09 s
4	4.45 s	4.33 s	23.84 s
5	4.33 s	4.33 s	21.66 s

**Table S2.** Mean run time for a test case<sup>a</sup> for each AIOMFAC-VISC mixing approach using a single CPU core<sup>b</sup>. See also Table S1.

Trial	aquelec	aquorg	ZSR
1	25.08 $\mu$ s	25.39 $\mu$ s	139.45 $\mu$ s
2	21.95 $\mu$ s	21.88 $\mu$ s	137.27 $\mu$ s
3	21.80 $\mu$ s	21.41 $\mu$ s	115.47 $\mu$ s
4	22.27 $\mu$ s	21.64 $\mu$ s	119.22 $\mu$ s
5	21.64 $\mu$ s	21.64 $\mu$ s	108.28 $\mu$ s

<sup>a</sup> The test case was 1:1 sucrose–Ca(NO<sub>3</sub>)<sub>2</sub> at  $a_w = 0.625$ ; see Fig. 11a.

<sup>b</sup> Processor: Intel(R) Core(TM) i5-6200U CPU @ 2.30GHz

## S3 Additional ternary and quaternary aqueous electrolyte mixtures

60 Figures S1 to S5 show additional data for ternary and quaternary aqueous electrolyte mixtures. See Table 4 for information on each data set.

## S4 Cation–anion parameter substitutions

When data are unavailable for certain cation–anion interactions, substitute values are used for the related parameters; see Table S3.

**Table S3.** Cation–anion pair substitutions in Table 7.

Missing Pair	Replacement Pair
$\text{Ca}^{2+}, \text{Br}^-$	$\text{Ca}^{2+}, \text{Cl}^-$
$\text{Mg}^{2+}, \text{Br}^-$	$\text{Mg}^{2+}, \text{Cl}^-$
$\text{Ca}^{2+}, \text{SO}_4^{2-}$	$\text{Mg}^{2+}, \text{SO}_4^{2-}$
$\text{Li}^+, \text{HSO}_4^-$	$\text{Li}^+, \text{Cl}^-$
$\text{K}^+, \text{HSO}_4^-$	$\text{K}^+, \text{Cl}^-$
$\text{NH}_4^+, \text{HSO}_4^-$	$\text{NH}_4^+, \text{Cl}^-$
$\text{Ca}^{2+}, \text{HSO}_4^-$	$\text{Ca}^{2+}, \text{Cl}^-$
$\text{Mg}^{2+}, \text{HSO}_4^-$	$\text{Mg}^{2+}, \text{Cl}^-$
$\text{NH}_4^+, \text{I}^-$	$\text{NH}_4^+, \text{Cl}^-$
$\text{Ca}^{2+}, \text{I}^-$	$\text{Ca}^{2+}, \text{Cl}^-$
$\text{Mg}^{2+}, \text{I}^-$	$\text{Mg}^{2+}, \text{Cl}^-$
$\text{Li}^+, \text{CO}_3^{2-}$	$\text{Na}^+, \text{CO}_3^{2-}$
$\text{Ca}^{2+}, \text{CO}_3^{2-}$	$\text{Mg}^{2+}, \text{SO}_4^{2-}$
$\text{NH}_4^+, \text{CO}_3^{2-}$	$\text{K}^+, \text{CO}_3^{2-}$
$\text{Mg}^{2+}, \text{CO}_3^{2-}$	$\text{Mg}^{2+}, \text{SO}_4^{2-}$
$\text{Li}^+, \text{HCO}_3^-$	$\text{Na}^+, \text{HCO}_3^-$
$\text{Ca}^{2+}, \text{HCO}_3^-$	$\text{Ca}^{2+}, \text{NO}_3^-$
$\text{NH}_4^+, \text{HCO}_3^-$	$\text{K}^+, \text{HCO}_3^-$
$\text{Mg}^{2+}, \text{HCO}_3^-$	$\text{Mg}^{2+}, \text{NO}_3^-$
$\text{Ca}^{2+}, \text{OH}^-$	$\text{Ca}^{2+}, \text{Cl}^-$
$\text{NH}_4^+, \text{OH}^-$	$\text{K}^+, \text{OH}^-$
$\text{Mg}^{2+}, \text{OH}^-$	$\text{Mg}^{2+}, \text{Cl}^-$
$\text{Li}^+, \text{IO}_3^-$	$\text{Li}^+, \text{NO}_3^-$
$\text{K}^+, \text{IO}_3^-$	$\text{K}^+, \text{NO}_3^-$
$\text{Na}^+, \text{IO}_3^-$	$\text{Na}^+, \text{NO}_3^-$
$\text{Ca}^{2+}, \text{IO}_3^-$	$\text{Ca}^{2+}, \text{NO}_3^-$
$\text{NH}_4^+, \text{IO}_3^-$	$\text{NH}_4^+, \text{NO}_3^-$
$\text{Mg}^{2+}, \text{IO}_3^-$	$\text{Mg}^{2+}, \text{NO}_3^-$

## 65 S5 Comparison of AIOMFAC-VISC when fitted with all data or only binary data

Figure S6 shows that some ternary and quaternary mixture predictions improve when these data are included in the fit, but mostly the results are similar. This suggests that viscosity measurements at higher concentrations, whether binary or multi-ion

mixtures, would be the most useful additions to the currently available measurements. Fortunately, droplet-based measurement techniques can probe concentration ranges outside of the bulk range.

## 70 **S6 Additional binary aqueous electrolyte curves**

Figures S7 – S10 show zoomed-in versions of Figs. 5 – 8. Figure S11 demonstrates the ability of the AIOMFAC-VISC model to capture a local viscosity minimum when only fitted to a single electrolyte. Figure S12 shows AIOMFAC-predicted water activity versus mass fraction of water for the binary aqueous nitrate solutions shown in Fig. 9. Figure S13 shows how AIOMFAC-VISC and the bulk measurements used to fit our model compare to droplet-based measurements from Power et al. (2013), which were not used to fit our model because they were not available in tabulated form. Note that the bulk measurements in Fig. S13 (aggregated by Laliberté (2007)) have significant spread between 293 and 298 K.

The scatter among similar measurement points is one reason for the inclusion of a 2 % uncertainty in viscosity applied to all bulk measurements. This is demonstrated by Fig. S14, which shows measurements and AIOMFAC-VISC predicted viscosities for temperatures between 268.15 K and 328.15 K.

## 80 **S7 Additional aqueous organic–inorganic viscosity predictions**

Richards et al. (2020b) included viscosity data for 1:1 organic–inorganic mixtures using a measurement technique described in Richards et al. (2020a). AIOMFAC-VISC predictions using the three mixing approaches described in Sect. 3.4 are shown in Figs. S15 and S16.

## **S8 Mixed $\alpha$ -pinene SOA + ammonium sulfate aerosol components**

85 The aerosol system discussed in Sect. 5 and featured in Figs. 12–14 is defined in Table S4.

**Table S4.** Components for  $\alpha$ -pinene SOA : ammonium sulfate containing aerosol with OIR = 1. Surrogate components for  $\alpha$ -pinene oxidation by ozone are derived from MCM, and their fixed dry amounts are given in mol m<sup>-3</sup> in the particulate matter (PM) phase.

Name (MCM)	O:C	<i>M</i> (g mol <sup>-1</sup> )	PM conc. (mol m <sup>-3</sup> )	SMILES
C107OOH	0.4	200.231	6.56 × 10 <sup>-11</sup>	O=CCC1CC(OO)(C(=O)C)C1(C)C
PINONIC	0.3	184.232	3.71 × 10 <sup>-11</sup>	OC(=O)CC1CC(C(=O)C)C1(C)C
C97OOH	0.44	188.22	7.55 × 10 <sup>-10</sup>	OCC1CC(OO)(C(=O)C)C1(C)C
C108OOH	0.5	216.231	2.52 × 10 <sup>-8</sup>	O=CCC(CC(=O)C(=O)C)C(C)(C)OO
C89CO2H	0.33	170.206	6.03 × 10 <sup>-12</sup>	O=CCC1CC(C(=O)O)C1(C)C
PINIC	0.444	186.205	2.41 × 10 <sup>-9</sup>	OC(=O)CC1CC(C(=O)O)C1(C)C
C921OOH	0.56	204.22	2.76 × 10 <sup>-9</sup>	OCC(=O)C1(OO)CC(CO)C1(C)C
C109OOH	0.4	200.231	4.72 × 10 <sup>-12</sup>	OCC(=O)C1CC(CC=O)C1(C)C
C812OOH	0.625	190.194	2.53 × 10 <sup>-9</sup>	OCC1CC(OO)(C(=O)O)C1(C)C
HOPINONIC	0.4	200.232	6.98 × 10 <sup>-10</sup>	OCC(=O)C1CC(CC(=O)O)C1(C)C
C811OH	0.375	158.094	2.68 × 10 <sup>-11</sup>	OCC1CC(C(=O)O)C1(C)C
C813OOH	0.75	206.193	9.89 × 10 <sup>-10</sup>	OCC(CC(=O)C(=O)O)C(C)(C)OO
ALDOL dimer	0.375	368.421	1.80 × 10 <sup>-10</sup>	CC(=O)C(=O)CC(C(C=O)=CCC1CC(C(O)=O)C1(C)C)C(C)(C)OO
ESTER dimer	0.375	368.421	7.20 × 10 <sup>-10</sup>	CC1(C)C(CC1C(O)=O)CC(=O)OCC(=O)C2CC(CC(O)=O)C2(C)C
(NH <sub>4</sub> ) <sub>2</sub> SO <sub>4</sub>	NA	132.14	5.89 × 10 <sup>-8</sup>	O=S([O-])([O-])=O.[NH4+].[NH4+]

The molar concentrations of the components in the PM phase ("PM conc.") are defined such that OIR = 1. However, under true atmospheric conditions, semi-volatile component concentrations would be expected to change, which would impact OIR. This table is adapted from Gervasi et al. (2020).

## References

- Fabuss, B. M., Korosi, A., and Othmer, D. F.: Viscosities of aqueous solutions of several electrolytes present in sea water, *Journal of Chemical & Engineering Data*, 14, 192–197, <https://doi.org/10.1021/je60041a025>, 1969.
- Gervasi, N. R., Topping, D. O., and Zuend, A.: A predictive group-contribution model for the viscosity of aqueous organic aerosol, *Atmospheric Chemistry and Physics*, 20, 2987–3008, <https://doi.org/10.5194/acp-20-2987-2020>, 2020.
- Goldsack, D. E. and Franchetto, A. A.: The viscosity of concentrated electrolyte solutions—III. A mixture law, *Electrochimica Acta*, 22, 1287–1294, [https://doi.org/10.1016/0013-4686\(77\)87012-6](https://doi.org/10.1016/0013-4686(77)87012-6), 1977.
- Iyoki, S., Iwasaki, S., Kuriyama, Y., and Uemura, T.: Densities, viscosities, and surface tensions for the two ternary systems water + lithium bromide + lithium iodide + lithium chloride + lithium nitrate, *Journal of Chemical & Engineering Data*, 38, 302–305, <https://doi.org/10.1021/je00010a031>, 1993.
- Laliberté, M.: Model for Calculating the Viscosity of Aqueous Solutions, *Journal of Chemical & Engineering Data*, 52, 321–335, <https://doi.org/10.1021/je0604075>, 2007.
- Nowlan, M.-F., Doan, T. H., and Sangster, J.: Prediction of the viscosity of mixed electrolyte solutions from single-salt data, *The Canadian Journal of Chemical Engineering*, 58, 637–642, <https://doi.org/10.1002/cjce.5450580514>, [\\_eprint: https://onlinelibrary.wiley.com/doi/pdf/10.1002/cjce.5450580514](https://onlinelibrary.wiley.com/doi/pdf/10.1002/cjce.5450580514), 1980.

- Power, R., Simpson, S., Reid, J., and Hudson, A.: The transition from liquid to solid-like behaviour in ultrahigh viscosity aerosol particles, *Chemical Science*, 4, 2597–2604, 2013.
- Richards, D. S., Trobaugh, K. L., Hajek-Herrera, J., and Davis, R. D.: Dual-Balance Electrodynamic Trap as a Microanalytical Tool for Identifying Gel Transitions and Viscous Properties of Levitated Aerosol Particles, *Analytical Chemistry*, 92, 3086–3094, 105 <https://doi.org/10.1021/acs.analchem.9b04487>, 2020a.
- Richards, D. S., Trobaugh, K. L., Hajek-Herrera, J., Price, C. L., Sheldon, C. S., Davies, J. F., and Davis, R. D.: Ion-molecule interactions enable unexpected phase transitions in organic-inorganic aerosol, *Science Advances*, 6, eabb5643, <https://doi.org/10.1126/sciadv.abb5643>, 2020b.
- Zhang, H.-L., Chen, G.-H., and Han, S.-J.: Viscosity and Density of H<sub>2</sub>O + NaCl + CaCl<sub>2</sub> and H<sub>2</sub>O + KCl + CaCl<sub>2</sub> at 298.15 K, *Journal of* 110 *Chemical & Engineering Data*, 42, 526–530, <https://doi.org/10.1021/je9602733>, 1997.

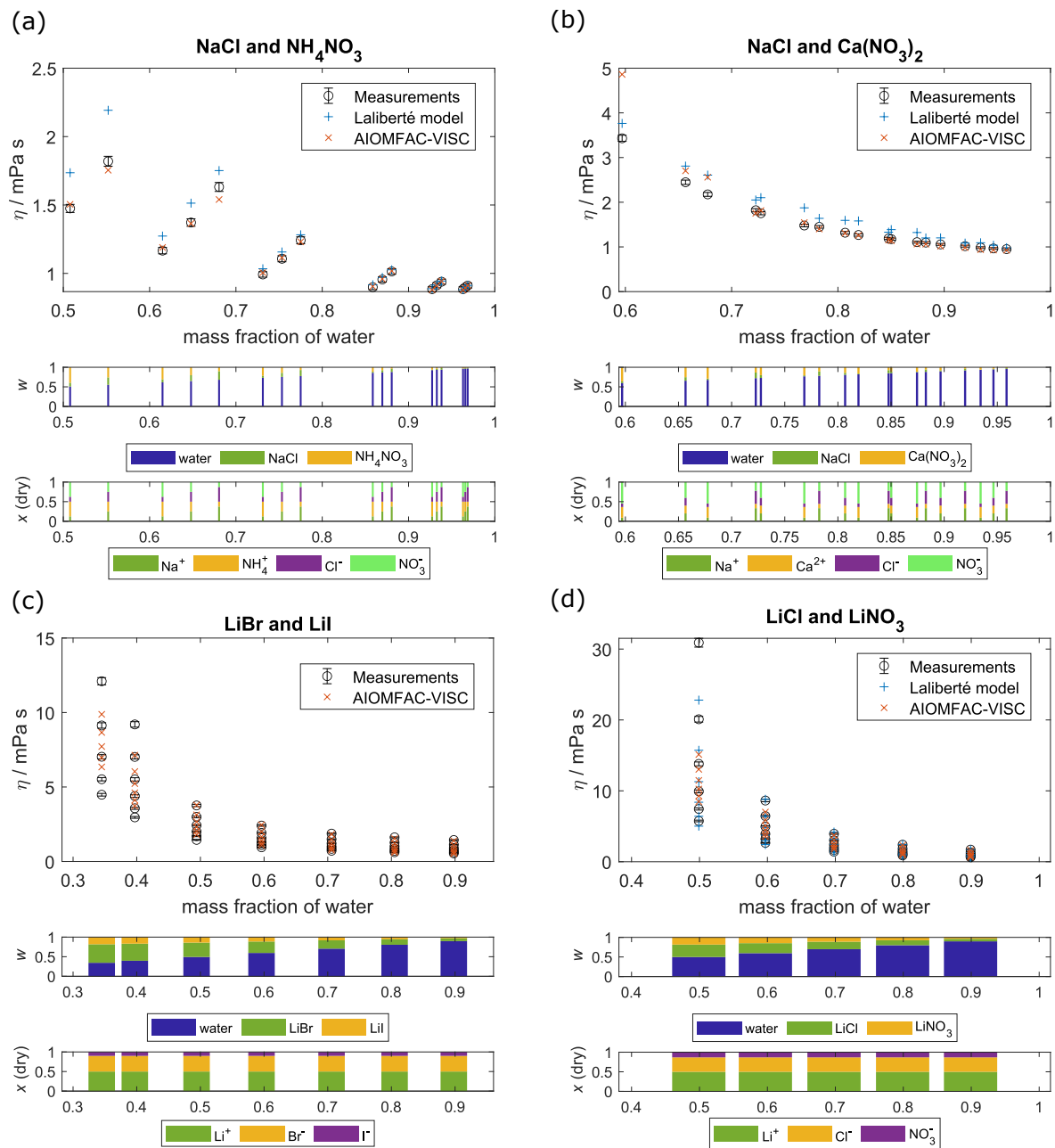


**Figure S1.** Comparison of AIOMFAC-VISC and the Laliberté model for ternary and quaternary aqueous electrolyte mixtures:(a) NaCl and  $\text{NH}_4\text{NO}_3$  (Nowlan et al., 1980); (b) NaCl and  $\text{Ca}(\text{NO}_3)_2$  (Nowlan et al., 1980); (c) LiBr and LiI (Iyoki et al., 1993); (d) LiCl and  $\text{LiNO}_3$  (Iyoki et al., 1993). Top panel: viscosity versus mass fraction of water with 2% error in viscosity included for all measurements. The Laliberté model does not offer predictions for LiBr or LiI, so the Laliberté model is not shown for (c). Middle panel: mass fractions of mixture input components. Bottom panel: mole fractions of ions in dry mixture.

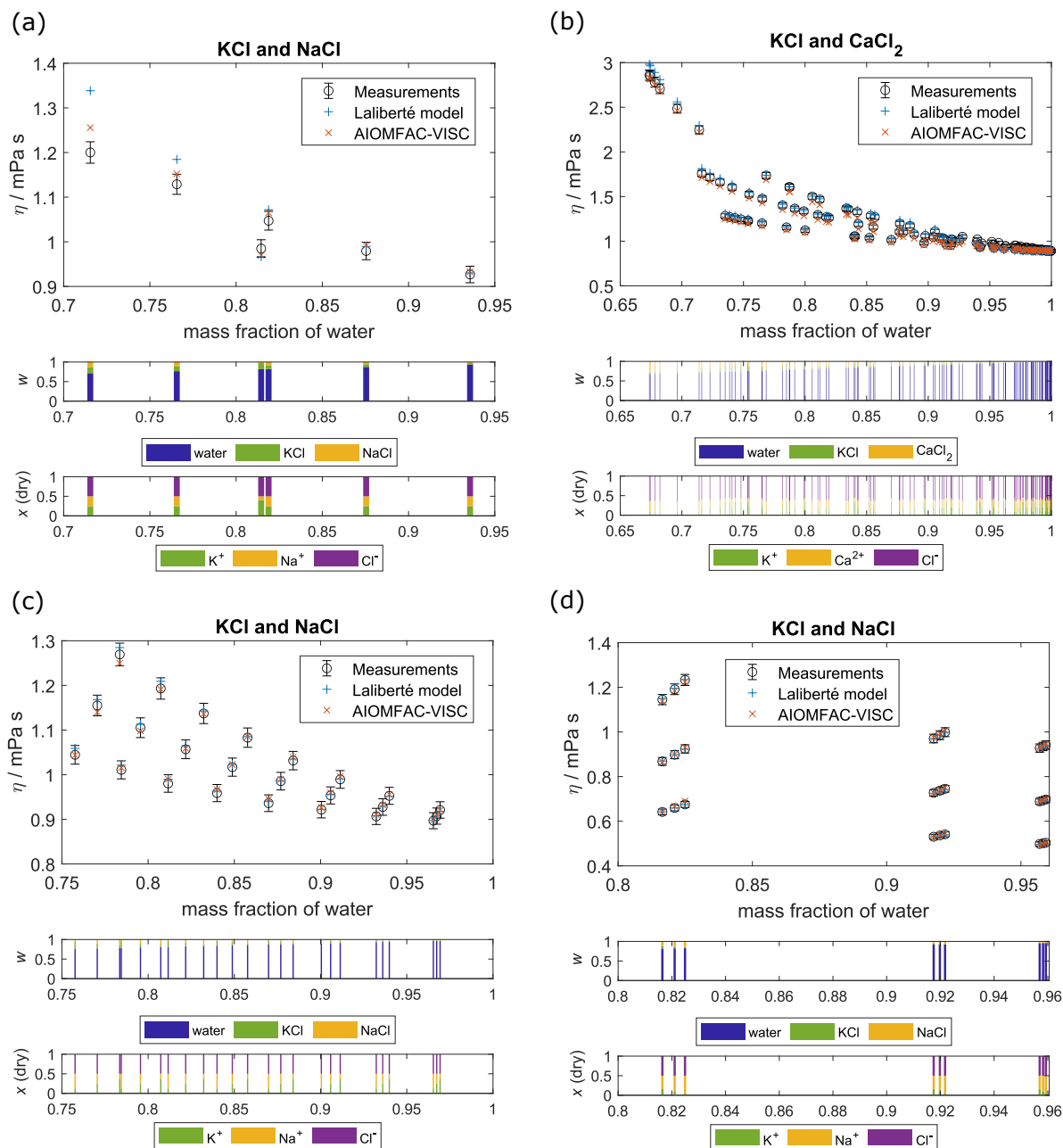


**Figure S2.** Comparison of AIOMFAC-VISC and the Laliberté model for ternary aqueous electrolyte mixtures: (a) KCl and NaCl (Goldsack and Franchetto, 1977); (b) KCl and  $\text{CaCl}_2$  (Zhang et al., 1997); (c) KCl and NaCl (Nowlan et al., 1980); (d) KCl and NaCl (Fabuss et al., 1969). Top panel: viscosity versus mass fraction of water with 2% error in viscosity included for all measurements. Middle panel: mass fractions of mixture input components. Bottom panel: mole fractions of ions in dry mixture.

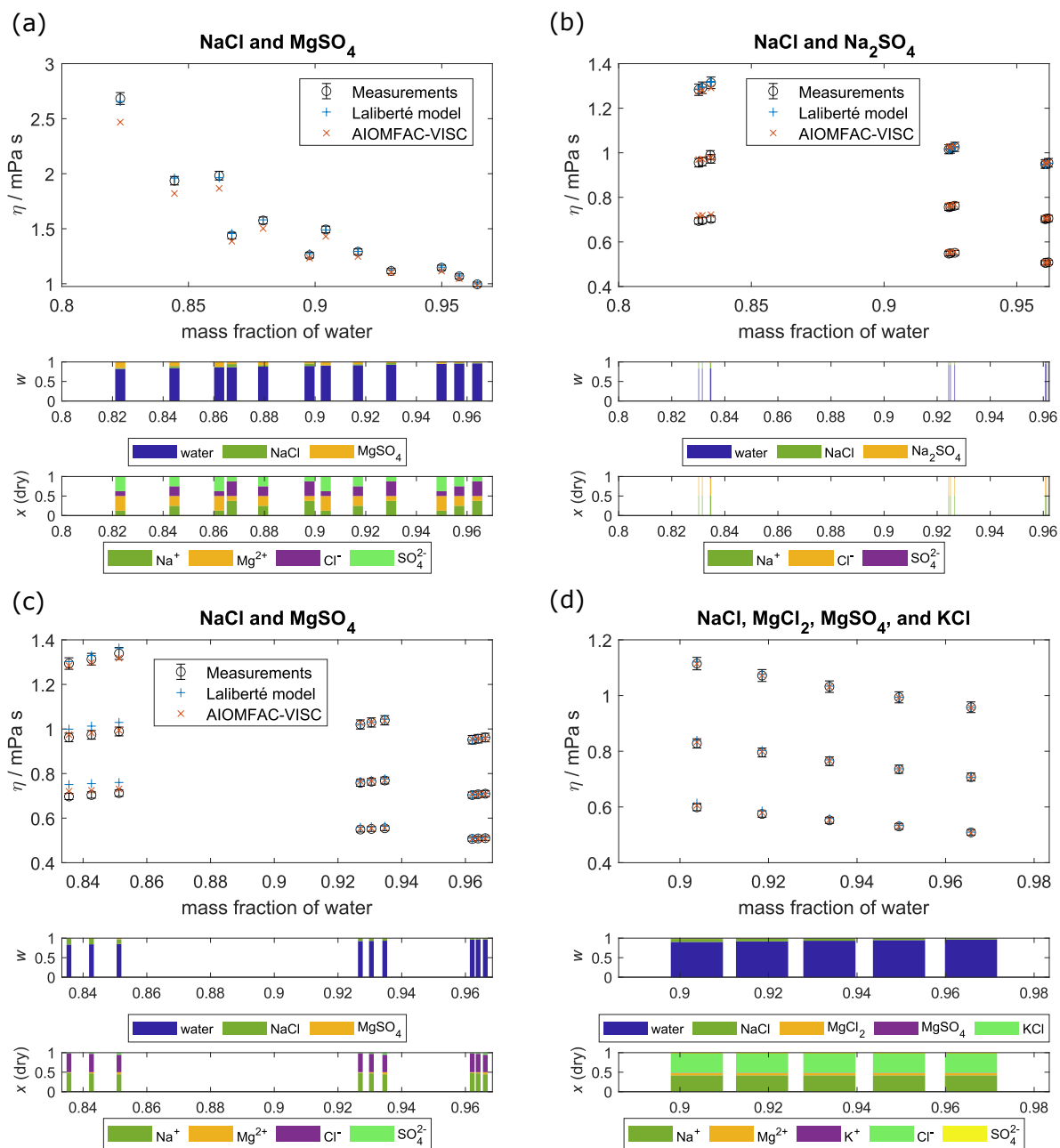


**Figure S3.** Comparison of AIOMFAC-VISC and the Laliberté model for ternary aqueous electrolyte mixtures: (a) NaCl and  $\text{MgSO}_4$  (Nowlan et al., 1980); (b) NaCl and  $\text{Na}_2\text{SO}_4$  (Nowlan et al., 1980); (c) NaCl and  $\text{MgSO}_4$  (Fabuss et al., 1969); (d) NaCl,  $\text{MgCl}_2$ ,  $\text{MgSO}_4$ , and KCl (Fabuss et al., 1969). Top panel: viscosity versus mass fraction of water with 2% error in viscosity included for all measurements. Middle panel: mass fractions of mixture input components. Bottom panel: mole fractions of ions in dry mixture.

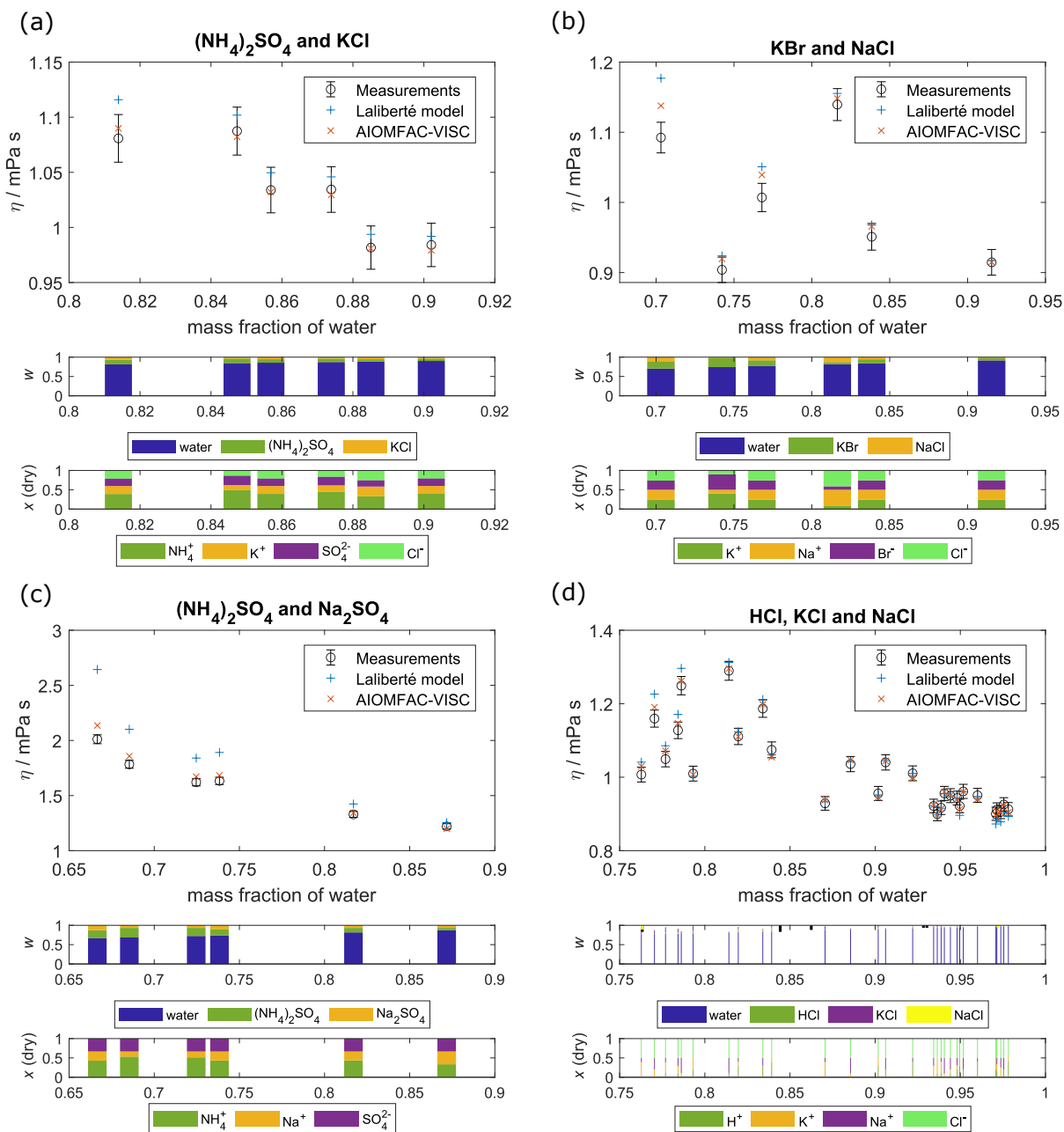


**Figure S4.** Comparison of AIOMFAC-VISC and the Laliberté model for ternary aqueous electrolyte mixture data from Goldsack and Franchetto (1977): (a)  $(\text{NH}_4)_2\text{SO}_4$  and KCl; (b) KBr and NaCl; (c)  $(\text{NH}_4)_2\text{SO}_4$  and  $\text{Na}_2\text{SO}_4$ ; (d) HCl, KCl and NaCl. Top panel: viscosity versus mass fraction of water with 2% error in viscosity included for all measurements. Middle panel: mass fractions of mixture input components. Bottom panel: mole fractions of ions in dry mixture.

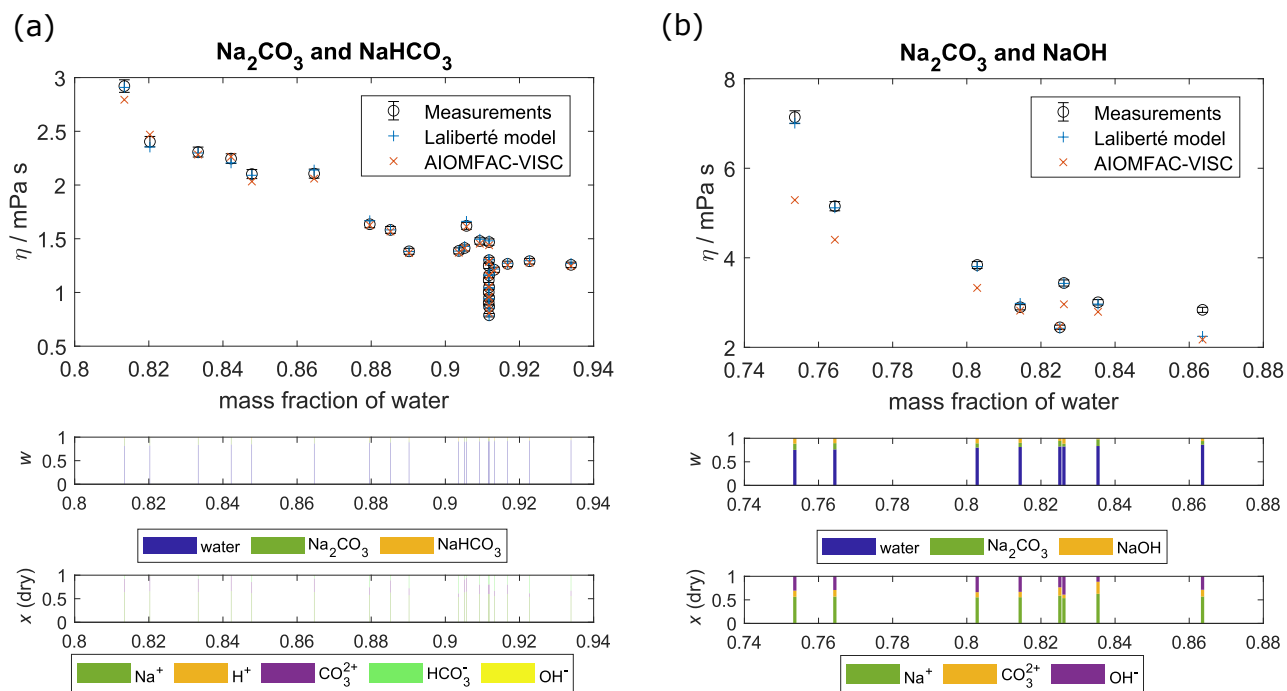


**Figure S5.** Comparison of AIOMFAC-VISC and the Laliberté model for ternary aqueous electrolyte mixture data aggregated by Laliberté (2007): (a)  $\text{Na}_2\text{CO}_3$  and  $\text{NaHCO}_3$ ; (b)  $\text{Na}_2\text{CO}_3$  and  $\text{NaOH}$ .

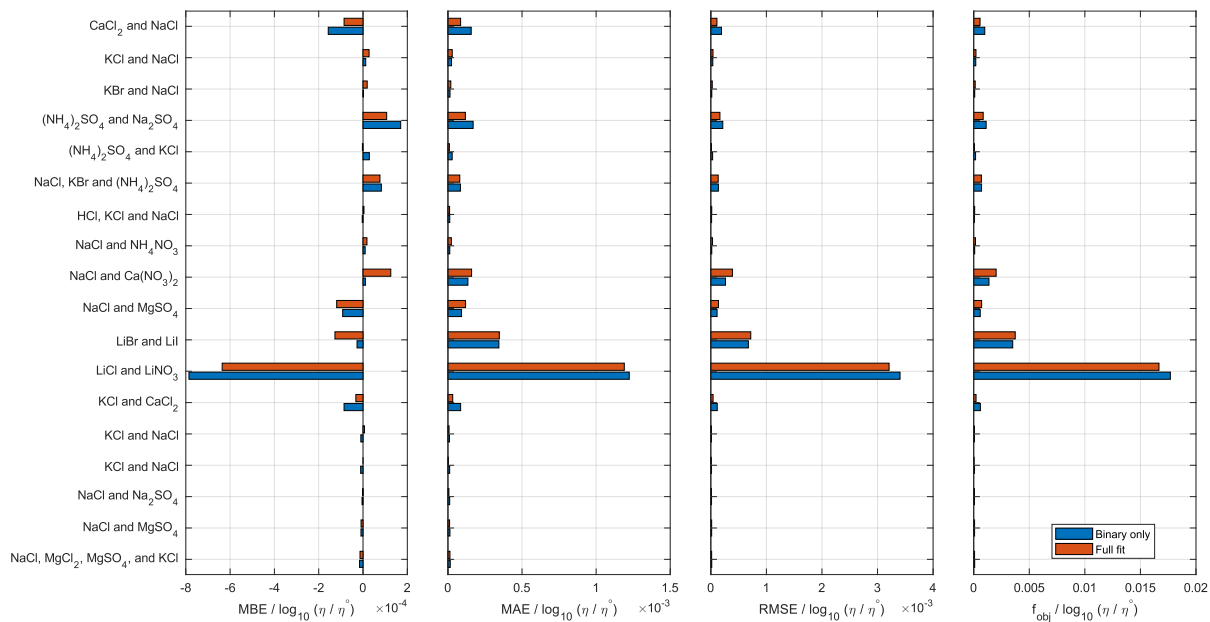


**Figure S6.** Comparison of the model–measurement error of AIOMFAC-VISC when using parameters fitted to only binary data (blue) versus to all available data (red): (a) mean bias error, (b) mean absolute error, (c) root mean square error, and (d) custom objective function value used to fit AIOMFAC-VISC. See Table 4 for information on number of data points, the ranges of temperature, concentration, and viscosity for each data set.  $\eta^\circ$  denotes unit viscosity (1 Pa s). See also Fig. 1.

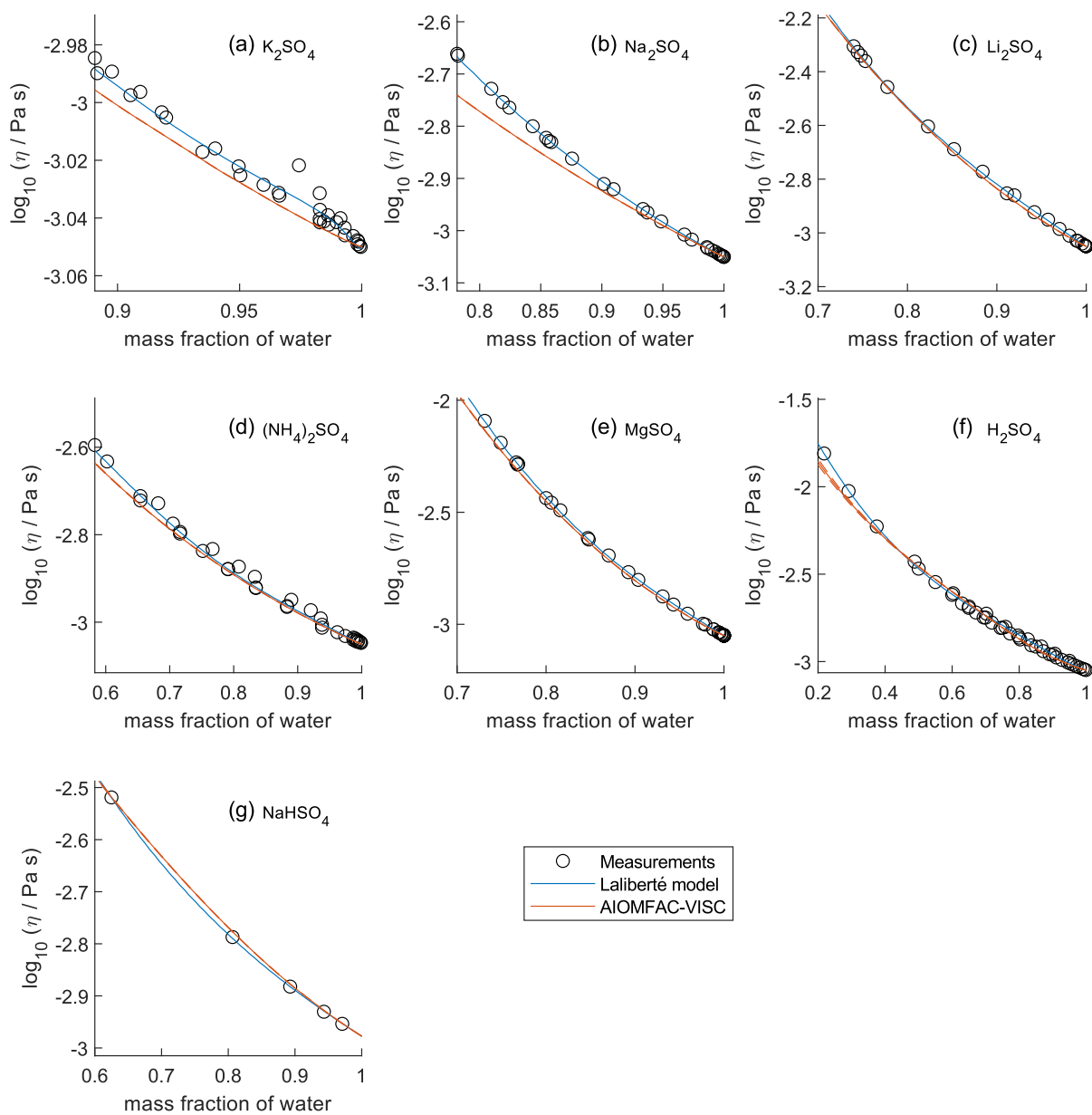


**Figure S7.** Comparison of the Laliberté model, AIOMFAC-VISC, and viscosity measurements versus mass fraction of water corresponding to Fig. 5. See also caption to Fig. 4.

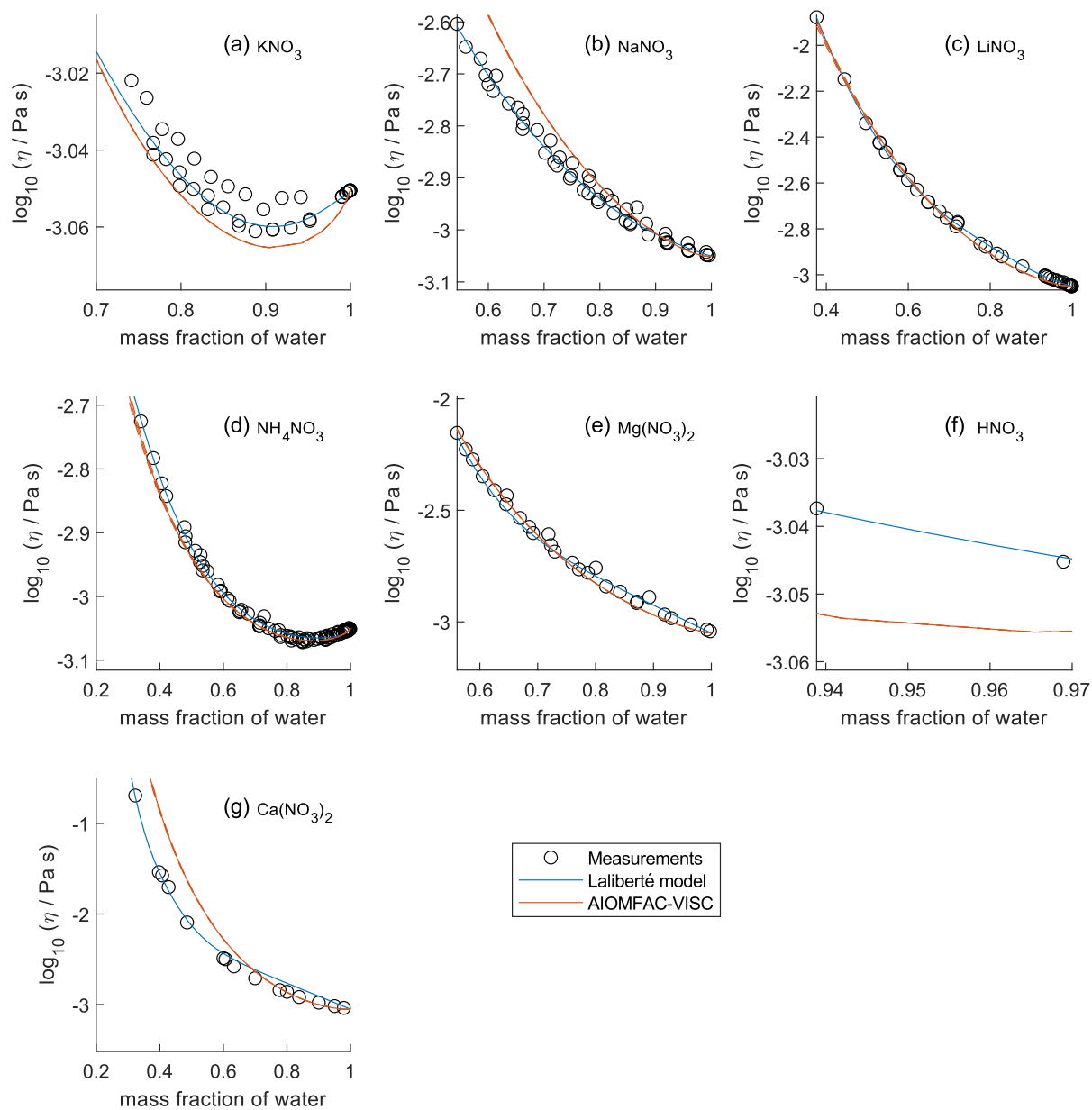


**Figure S8.** Comparison of the Laliberté model, AIOMFAC-VISC, and viscosity measurements versus mass fraction of water corresponding to Fig. 6. See also caption to Fig. 4.

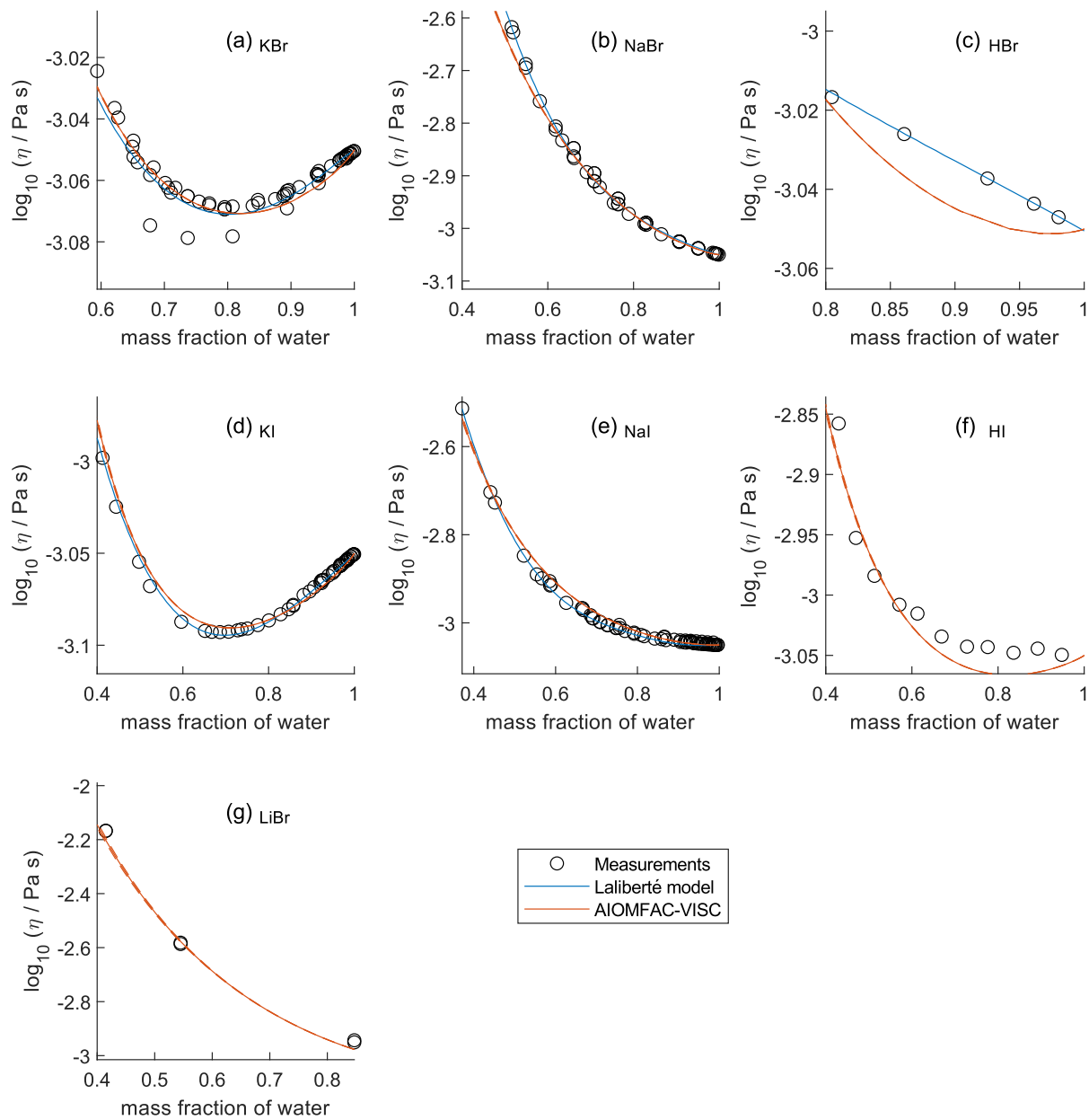


**Figure S9.** Comparison of the Laliberté model, AIOMFAC-VISC, and viscosity measurements versus mass fraction of water corresponding to Fig. 7. See also caption to Fig. 4.

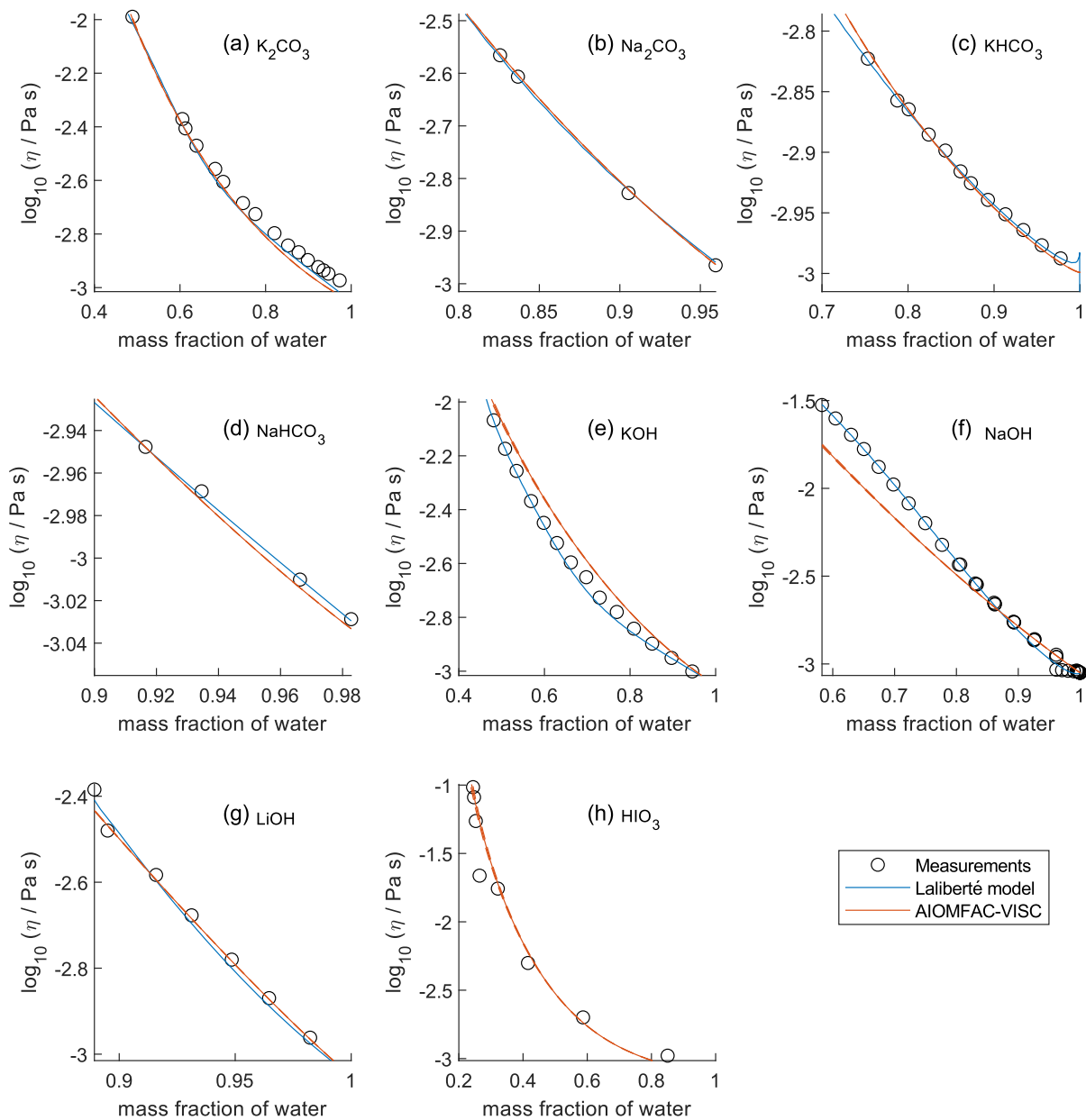


**Figure S10.** Comparison of the Laliberté model, AIOMFAC-VISC, and viscosity measurements versus mass fraction of water corresponding to Fig. 8. See also caption to Fig. 4.

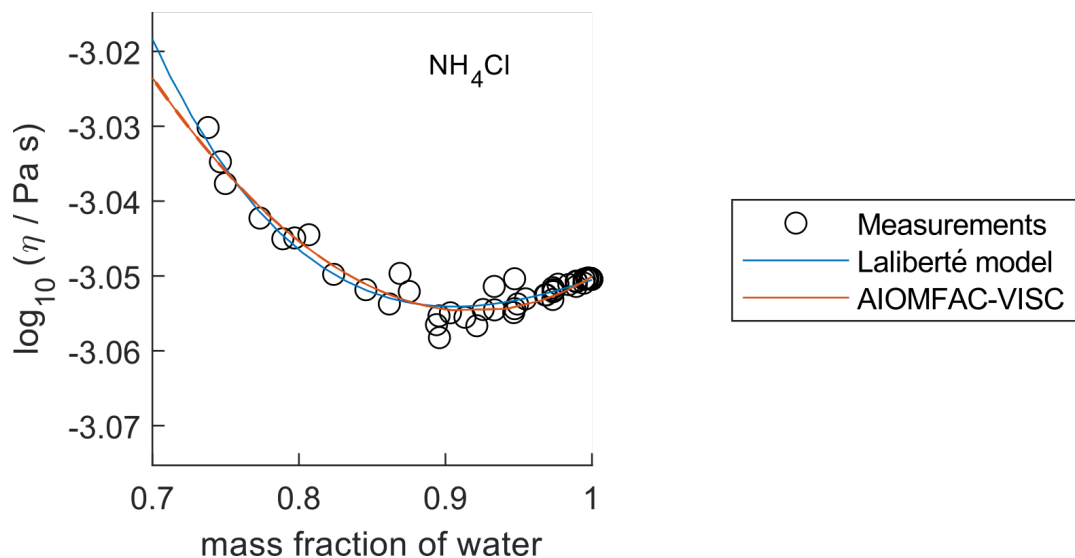


**Figure S11.** Comparison of the Laliberté model, AIOMFAC-VISC, and viscosity measurements versus mass fraction of water for  $\text{NH}_4\text{Cl}$  at 298 K when only binary  $\text{NH}_4\text{Cl}$  at 298 K was used to fit the model. Compare to result of simultaneous fit shown in Fig. 2d.

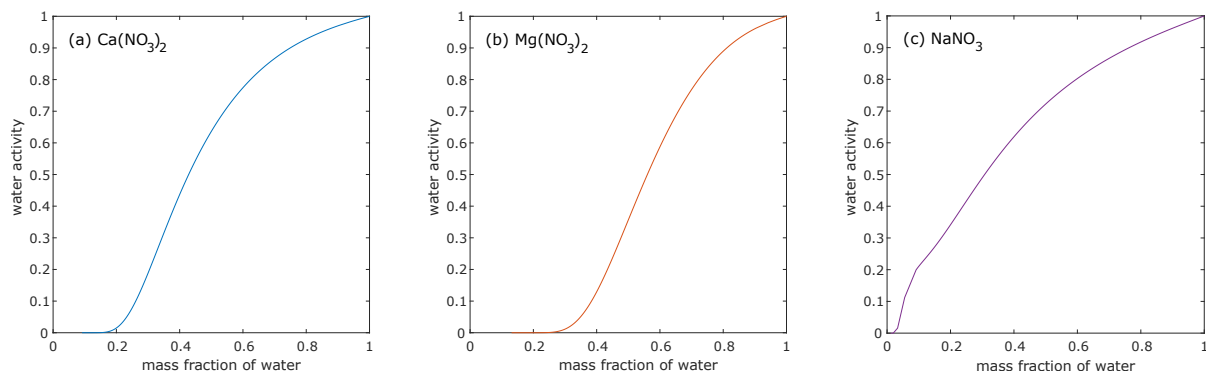


**Figure S12.** Mass fraction of water versus AIOMFAC-predicted water activity for binary aqueous nitrate solutions. Panels correspond to those of Fig. 9.

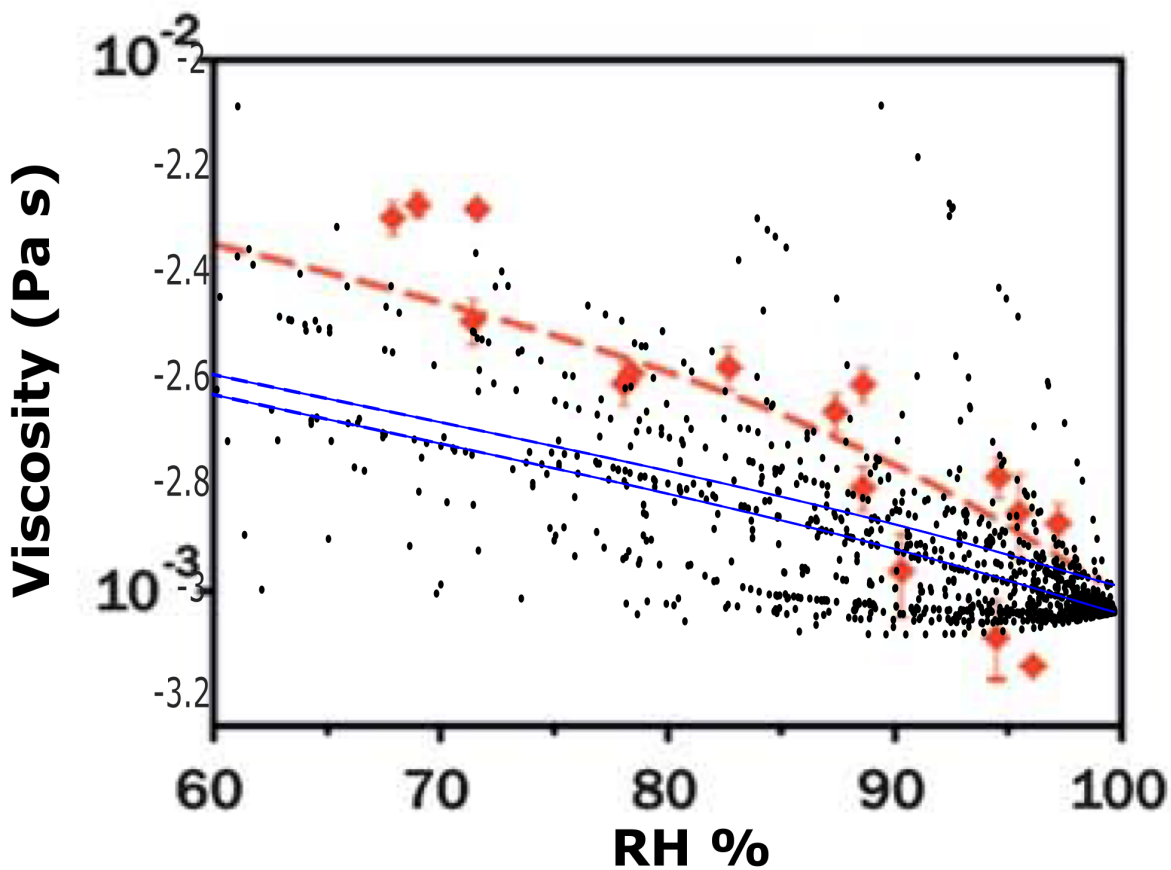


**Figure S13.** AIOMFAC-predicted viscosity for binary NaCl (blue solid curves) and bulk measurements (black dots) overlaid on droplet-based measurements (red diamonds) and ADDEM model prediction (red dashed curve) from the inset of Fig. 3a in Power et al. (2013). Power et al. (2013) state that their measurements were completed at “room temperature” but do not otherwise specify the precise temperature, so we have included bulk measurements from 293 to 298 K and AIOMFAC-VISC model curves for 293 and 298 K as upper and lower bounds, respectively.

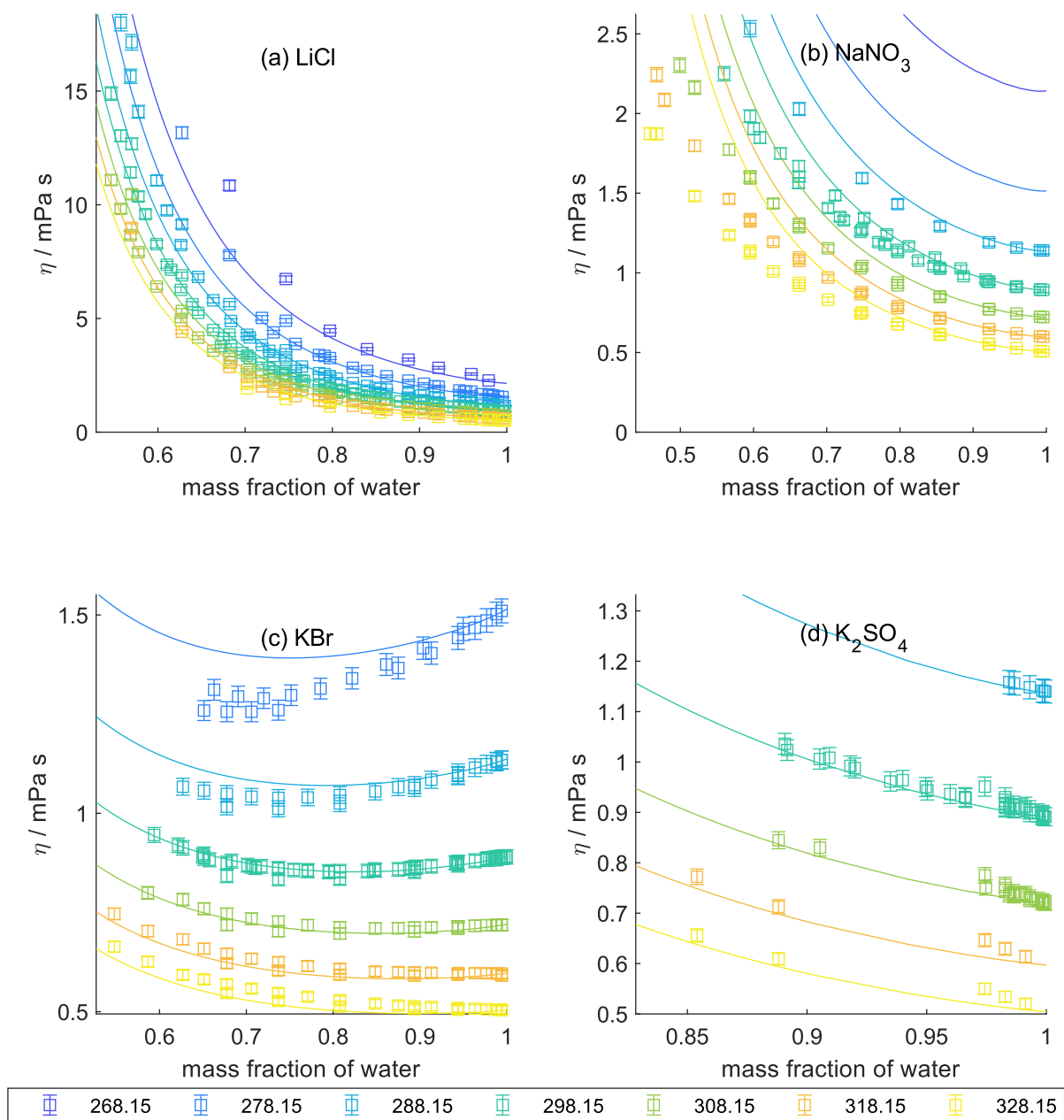


**Figure S14.** Viscosity measurements aggregated by Laliberté (2007) for a selection of binary aqueous solutions at several temperatures between 268.15 and 323.15 K: (a) LiCl; (b) NaNO<sub>3</sub>; (c) KBr; (d) K<sub>2</sub>SO<sub>4</sub>. 2 % viscosity error bars are included to account for scatter among similar measurement points. Solid lines are AIOMFAC-VISC predictions.

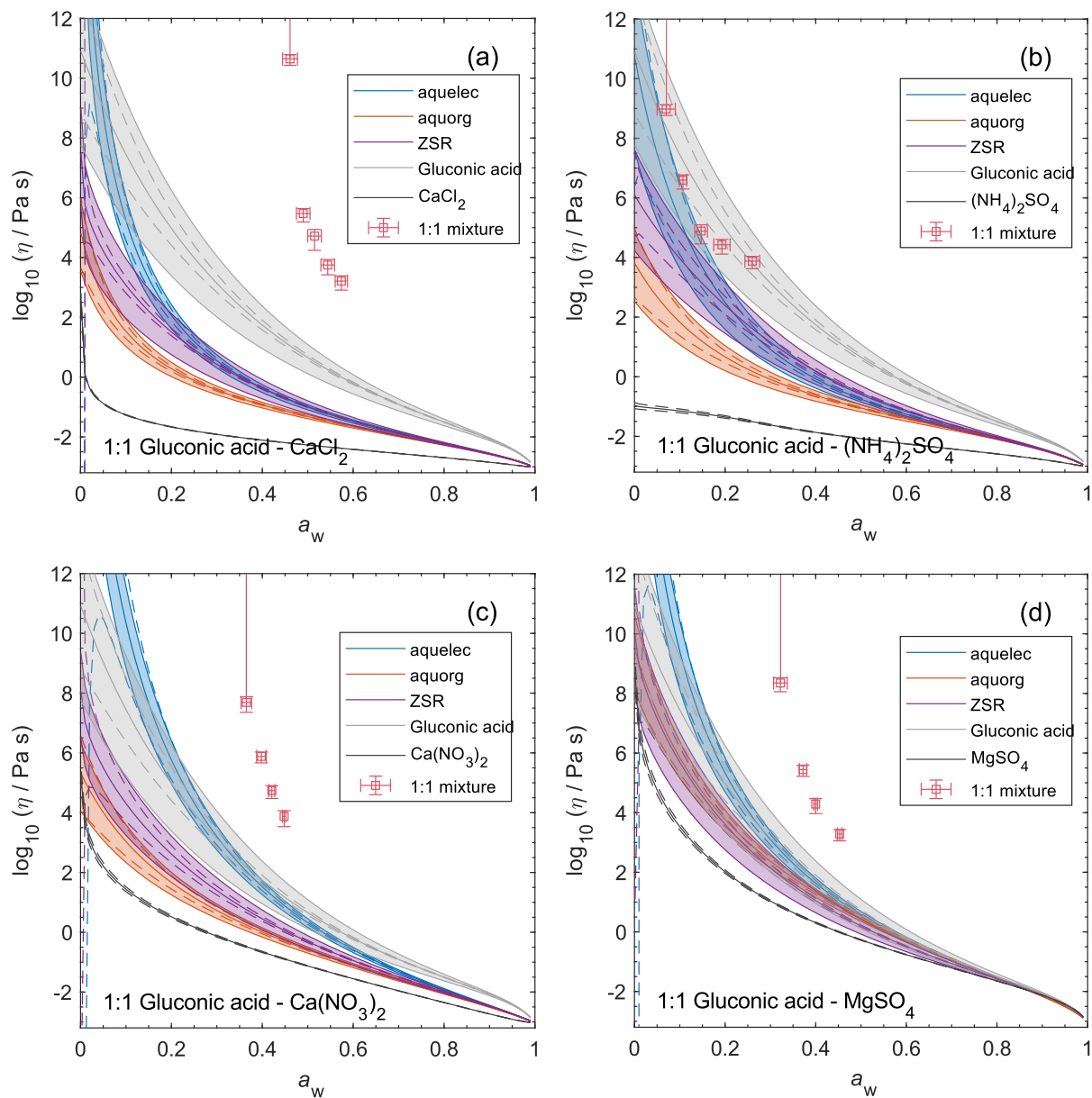


**Figure S15.** Viscosity predictions for aerosol surrogate mixtures containing gluconic acid and divalent salts at varying water activity,  $a_w$  (RH), with a prescribed organic-to-inorganic dry mass ratio (OIR). Three mixing models – aquelec, aquorg, and ZSR – are shown alongside the viscosity measurements. Model sensitivity, defined by the impact of a  $\pm 2\%$  change in aerosol water content, is shown by the dashed curves. Shaded regions show the potential viscosity prediction error introduced by a  $\pm 5\%$  error in the (estimated) glass transition temperature of the organic component. AIOMFAC-VISC predictions are also included for the binary aqueous sucrose and aqueous salt systems, which correspond to the organic and inorganic subsystems used in each mixing model (see Section 3.4). Model–measurement deviations for the organic–salt mixtures are likely due to a phase transition, such as gel formation.

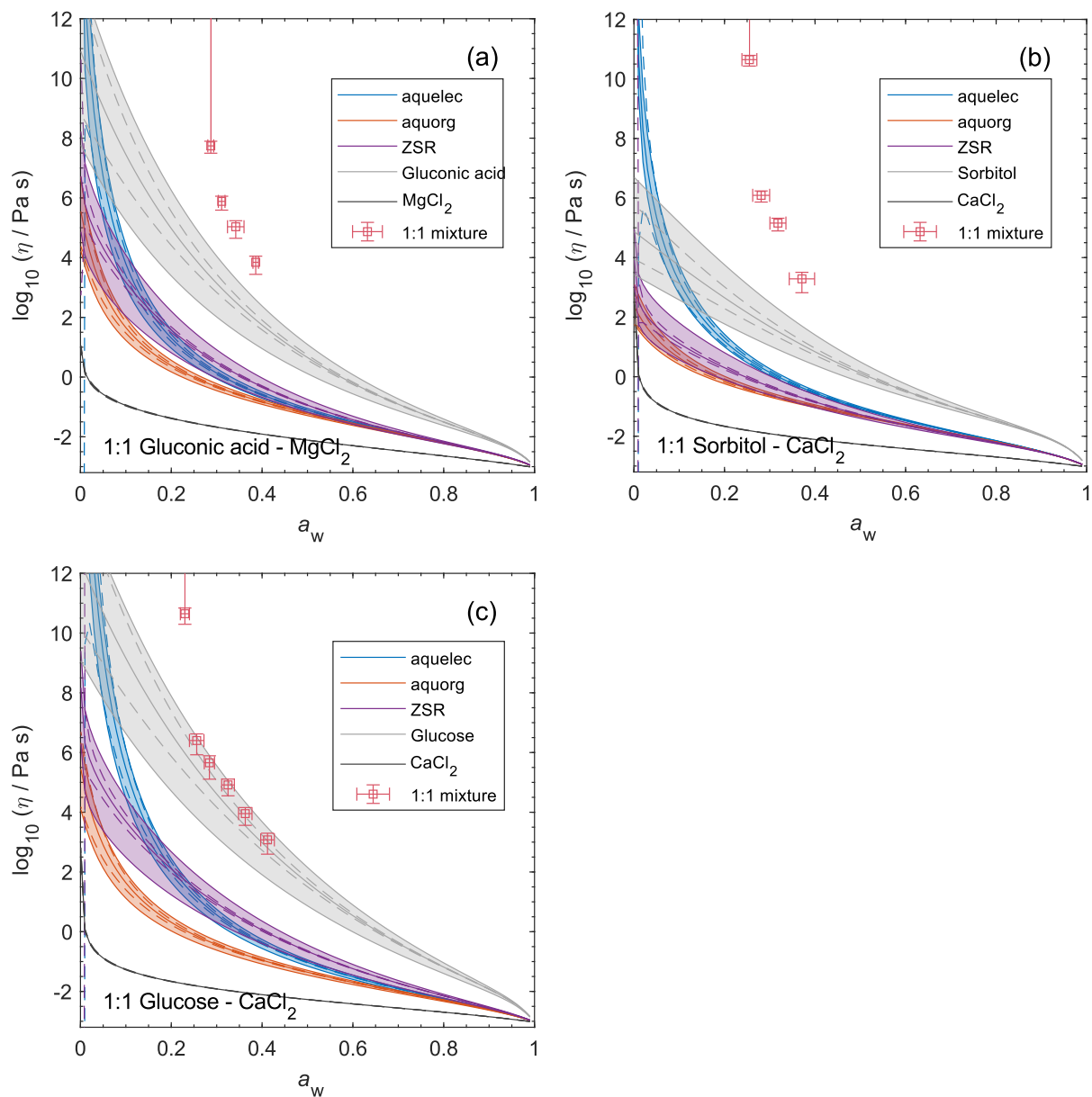


**Figure S16.** Viscosity predictions for aerosol surrogate mixtures containing organic compounds and divalent ions/salts at varying water activity,  $a_w$  (RH), with a prescribed organic-to-inorganic dry mass ratio (OIR). See also caption to Fig. S15.